Thermophoresis-Brinkman flow of an aerosol particle within a spherical cavity

M.S. Faltas [a] E.I. Saad [b,*]

[a] *Department of Mathematics, Faculty of Science, Alexandria University, Alexandria, Egypt*

[b] *Department of Mathematics, Faculty of Science, Damanhour University, Damanhour, Egypt*

Abstract

A semi-analytical study is presented for the thermophoretic migration of a spherical particle located at an arbitrary position in a porous medium inside a spherical cavity. A uniform applied temperature gradient parallel to the line connecting the particle and cavity centres. The porous medium is modeled as a Brinkman fluid with a characteristic Darcy permeability K that can be obtained directly from the experimental data. The porous medium is assumed to be homogenous, isotropic and the solid matrix is in thermal equilibrium with the fluid through the voids of the medium. The Knudsen number is supposed to be small so that the fluid flow through the porous medium can be described by a continuum model with a temperature jump, a thermal creep, a frictional slip and thermal stress slip at the surface of the aerosol particle. The Reynolds number of the fluid is assumed to be small enough to justify the use of the Brinkman equation, which is always satisfied because the aerosol particle is so small. The Péclet number for heat transfer in thermophoresis is also assumed to be small. The dimensionless thermophoretic velocity and the mobility coefficients are tabulated and represented graphically for various values of the permeability parameter, relative thermal and surface properties of the particle and cavity. Results are in good agreement with the analytical solution of the particular case of a particle located at the centre of the cavity.

Key words: Brinkman flow; thermophoresis; frictional and thermal slip; collocation technique; wall effect.

1. Introduction

The thermophoretic force is the force acting on particles embedded in a fluid due to a temperature gradient. The direction of the force is opposite to the temperature gradient. This anomaly was first observed by Tyndall [1]; he observed that a particle free zone around a heated surface appeared in dusty air. The thermophoretic effect can

* Corresponding author. E.I. Saad
Email address: elssaad@sci.dmu.edu.eg (E.I. Saad).

be explained by using the kinetic theory of gases [2]. The anomaly where particles are affected by the thermophoretic force is called thermophoresis. There are many applications of thermophoresis and cases where this effect is of considerable importance, e.g. filters, particle deposition on boilers and different measurement techniques for aerosols during combustion and its sampling [3], cleaning of air [4], scale formation on surfaces of heat exchangers [5], modified chemical vapor deposition [6], micro-electronic manufacture [7], and nuclear reactor safety [8].

In many biological and engineering applications a fluid can be treated as a continuum, that is only the overall motion of the particles is considered and not the individual motion of every particle, then The Brinkman equation for the fluid flow through the voids of a porous medium and Fourier law for the thermal flow can be used. However, in gases if the size of the embedded particle in the gas is small compared to the mean free path of the gas, ℓ, the gas cannot be treated as a continuum. Therefore, in such cases, the gas may be considered as rarefied and we must use the Boltzmann equation. That has happened when a microscopic particle embedded in a gas or when the gas has very high mean free path. The ratio between the mean free path of the gas and the characteristic length, a of the immersed particle, is defined as the Knudsen number, i.e.,

$$K_n = \frac{\ell}{a}. \tag{1.1}$$

The relevant flow and heat transfer models depend on the range of the Knudsen number. A classification of the different flow regimes is given in [9,10]: for $K_n \leq 0.01$ the fluid can be treated as a continuum, while for $K_n \geq O(10)$ it is treated as a free-molecular flow. A rarefied gas can be treated neither an absolutely continuous medium, nor a free-molecular flow in the Knudsen number range between 0.01 and 10. In that region, a further division is required: slip flow ($0.01 < K_n < 0.1$), and transition flow ($0.1 < K_n < 10$). This categorization is based on empirical knowledge and thus the limits between the different flow regimes may depend on the problem geometry.

Thermophoresis in a porous media is of specific importance in the branches of environmental and biomedical engineering [11–14]. The porous medium through which thermophoresis occur is modeled as an effective Brinkman medium. To model the fluid flow through the voids of a porous medium, Brinkman [15] first add an extra term, which represents the hydraulic drag force induced by the presence of the solid matrix within a porous medium into the Navier-Stokes equation, the new equation is called the Brinkman equation. The hydrodynamic permeability of this medium can be characterized by the Darcy permeability K. In spite of the Brinkman equation is semiempirical, it is in a good agreement with the experimental data in general [16] and is considered as a standard means to describe the fluid flow through a porous medium. In the literature, it is reported that the Brinkman model is generally applicable to describe the fluid flow in all kinds of porous media, e.g. the polymer gel in DNA sequencing techniques [17].

Under the conditions of small Knudsen, small Péclet number, and small Reynolds number, with the effects of temperature jump, thermal creep, frictional slip, and thermal stress slip at the surface of a spherical particle embedded in a Brinkman medium with

constant temperature gradient ∇T_∞, the thermophoretic velocity is given by [18]

$$\vec{U}_0 = -\frac{\mu}{\rho_A T_0}\left[\frac{18(\alpha+1)\Big(\big[k_A+(\tilde{C}_t-1)\,k_p\big]\,C_h\,\tilde{C}_m + C_s\,(\tilde{C}_t\,k_p+k_A)\Big)}{\Big(2k_A+(2\tilde{C}_t+1)\,k_p\Big)\Big((\alpha^3+3\alpha^2+18\alpha+18)\,\tilde{C}_m+\alpha^2+9\alpha+9\Big)}\right]\nabla T_\infty. \tag{1.2}$$

In the expression (1.2), ρ_A and k_A are the overall density and overall thermal conductivity, respectively, of the porous medium, μ is the density of the fluid through porous medium, k_p is the thermal conductivity of the particle, and T_0 represents the temperature at the centre of the particle or the mean temperature of the porous medium in the vicinity of the particle. The dimensionless quantities $\tilde{C}_t$ and $\tilde{C}_m$ are defined respectively by $\tilde{C}_t = C_t\ell/a$ and $\tilde{C}_m = C_m\ell/a$, respectively, where a is the radius of the particle. The dimensionless coefficients C_t, C_s, C_m and C_h are, respectively, the temperature jump, the thermal creep, frictional slip and thermal stress slip; theses coefficients have to determined experimentally for various fluid/solid system. The permeability parameter α is defined in terms of Darcy permeability K as $a/\sqrt{K}$. In the view of kinetic theory of gases and experimental studies, reliable values for thermal jump and slip coefficients are as follows [19–24]: $C_t = 2.0 \sim 2.3$, $C_s = 1.0 \sim 1.3$, $C_m = 1.0 \sim 1.5$ and $C_h = 1.0 \sim 3.0$. As $\alpha = 0$ (i.e., clear Stokes flow), equation (1.2) becomes the well-known formula obtained by Chang and Keh [25].

In actual applications of thermophoresis in microfluidic equipment, the size of the aerosol particles and confining boundaries are proportionate, and it is necessary to find out if the closeness of the boundary wall essentially effects the particle mobility [26]. In literature, the interaction problems of thermophoretic effect in the presence of wall boundaries were studied extensively [27–31]. Some of these investigations include the second order temperature gradient in the slip flow regime at solid boundaries [32–35]. Recently, Tseng and Keh [36] studied the problem of thermophoresis of an aerosol sphere located arbitrarily in a spherical cavity normal to the line of their centers in the slip-flow regime. They found that the wall effect on the thermophoretic migration normal to the line through the particle and cavity centers is slightly weaker than that along the line. The problem of spherical particle moving in a spherical cavity can be considered as a model for the capture of ash particles undergoing thermophoresis in porous filters composed of connecting spherical pores.

The purpose of this article is to study and find a correction to (1.2) of the thermophoretic velocity of an aerosol spherical particle located arbitrarily within a spherical cavity subject to a prescribed temperature gradient parallel to the line connecting their centers. We use the Brinkman equation with the effective viscosity equal to the bulk value to analyze the flow inside the porous cavity. The temperature and fluid velocity fields satisfying the Laplace and Brinkman equations, respectively, are determined utilizing the technique of boundary collocation. This problem is an extension of the work by Cheng and Keh [33] to the case of porous medium saturated by a viscous fluid. The novelty of this problem is to study the effect of permeability of the porous medium and the wall effect on thermophoretic velocity. Low and high permeabilities are also investigated.

2. Equation of heat transfer through a porous medium

In the following analysis, we append the subscripts s and f, respectively, for the solid and fluid phases. Therefore, the overall density ρ_A and overall thermal conductivity k_A are, respectively, defined as

$$\rho_A = (1-\varphi)\,\rho_s + \varphi\,\rho_f, \tag{2.1}$$
$$k_A = (1-\varphi)\,k_s + \varphi\,k_f, \tag{2.2}$$

where φ is the porosity. Nield and Bejan [37], developed an equation describing the steady state of the temperature distribution T through an isotropic homogenous porous medium by taking averages over an elemental volume of the medium in the absence of overall heat production per unit volume of the medium:

$$\nabla \cdot k_A \nabla T = 0, \tag{2.3}$$

In equation (2.3), the following assumptions are made: at every point in the porous medium, the solid matrix is in thermal equilibrium with the fluid through the voids of the medium, $T_s = T_f = T$, the radiative effects, viscous dissipation, and the work done by pressure changes are not included. The Péclet number of the fluid phase is assumed to be small such the convection term can be neglected. In general, the overall thermal conductivity of a porous medium depends on the microstructure and geometry of the medium. The definition (2.1) of the overall thermal conductivity based on the fact that, the heat conduction in the solid and fluid phases occurs in parallel. However, if the structure and orientation of the porous medium is such that the heat conduction takes place in series, with all of the heat flux passing through both solid and fluid, then the overall conductivity k_H is the weighted harmonic mean of k_s and k_f:

$$\frac{1}{k_H} = \frac{\varphi}{k_s} + \frac{1-\varphi}{k_f}, \tag{2.4}$$

In general, k_A and k_H will provide upper and lower bounds, respectively, on the actual overall conductivity. Other discussions on overall thermal conductivity can be found in the book of Neild and Bejan [37].

3. Description of the problem

Consider the axially symmetric thermophoretic motion of a spherical particle of radius a suspended at an arbitrary position within a spherical cavity of radius b filled with a porous medium, saturated by a gaseous flow at the quasisteady state. Let (r_1, θ_1, ϕ) and (r_2, θ_2, ϕ) be two systems of spherical coordinates with origins located at the centres of the particle and cavity, respectively, with corresponding unit vectors $(\vec{e}_{r_1}, \vec{e}_{\theta_1}, \vec{e}_{\phi})$ and $(\vec{e}_{r_2}, \vec{e}_{\theta_2}, \vec{e}_{\phi})$. The center of the particle is situated away from the center of the cavity along the z-axis at a distance d instantaneously. Let also (ρ, ϕ, z) be a system of cylindrical coordinates with origin at the centre of the cavity and with corresponding unit vectors

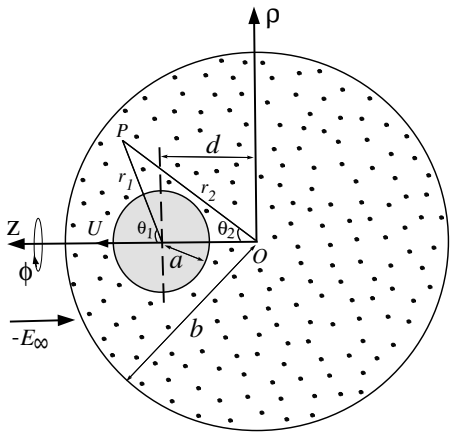

Fig. 1. Coordinate graph for the thermophoresis of an aerosol sphere in a spherical cavity.

$(\vec{e}_\rho, \vec{e}_\phi, \vec{e}_z)$ as illustrated in Fig. 1. The relation between the two systems of spherical coordinates is given by

$$r_1^2 = r_2^2 + d^2 - 2\, r_2\, d\, \cos\theta_2, \tag{3.1}$$

or by

$$r_2^2 = r_1^2 + d^2 + 2\, r_1\, d\, \cos\theta_1. \tag{3.2}$$

A constant temperature gradient, $-E_\infty\, \vec{e}_z = \nabla T_\infty\, (E_\infty > 0)$ is maintained far from the particle and in the vicinity of the cavity. Clearly, T_∞ is a linear relation with $z : T_\infty = T_0 - E_\infty\, z$. Let $\vec{U} = U\, \vec{e}_z\, (U > 0)$ be the velocity of the particle to be determined. We assume that the solids that comprised the porous medium is uniformly distributed in the system. The hydrodynamic permeability of the porous medium can be characterized by the Darcy permeability K so that the friction coefficient γ can be expressed as μ/K. The fluid through the voids of the porous medium is incompressible and Newtonian, is allowed to slip, both thermally and frictionally at the surface of the particle and cavity, and the temperature jump may occur at the particle surface. Gravitational effects are ignored. Our aim here is to determine the correction to equation (1.2) for the particle velocity due the presence of the cavity. We assume also that the thermal properties of the particle and porous medium are constants and that the Knudsen number is in the range of the slip-flow regime. In the following two subsections, we first consider the thermal distribution analysis and then the hydrodynamical flow analysis through the porous medium.

3.1. Analysis for thermal distributions

According to the assumptions stated in previous sections, the energy equations governing the temperature distributions, T_p of the particle $(r_1 \le a)$, T of the porous region

($r_1 \geq a$, $r_2 \leq b$), and T_w of the region outside the cavity ($r_2 \geq b$) are given, respectively, as

$$\nabla^2 T_p = 0, \tag{3.3}$$
$$\nabla^2 T = 0, \tag{3.4}$$
$$\nabla^2 T_w = 0. \tag{3.5}$$

The boundary conditions at the particle and cavity surfaces require that, the normal heat fluxes to be continuous and a temperature jump, which is proportional to the normal temperature gradient [2] to occur. Also, the fluid temperature must approach the linear prescribed field far away from the particle and the temperature inside the particle is finite everywhere. Thus, we obtain

$$k_A \frac{\partial T}{\partial r_1} = k_p \frac{\partial T_p}{\partial r_1}, \quad \text{at } r_1 = a, \tag{3.6}$$
$$k_A \frac{\partial T}{\partial r_2} = k_w \frac{\partial T_w}{\partial r_2}, \quad \text{at } r_2 = b, \tag{3.7}$$
$$T - T_p = C_t \ell \frac{\partial T}{\partial r_1}, \quad \text{at } r_1 = a, \tag{3.8}$$
$$T - T_w = -\breve{C}_t \ell \frac{\partial T}{\partial r_2}, \quad \text{at } r_2 = b, \tag{3.9}$$
$$T_p \text{ is finite in } r_1 < a, \tag{3.10}$$
$$T_w \to T_\infty = T_0 - E_\infty z, \quad \text{as } r_2 \to \infty, \tag{3.11}$$

where k_w denotes the constant thermal conductivity of the cavity surface, $\breve{C}_t$ is the dimensionless temperature jump coefficient, which depends on the nature of the fluid through the porous medium and the material of cavity wall. The temperature jump coefficient, $\breve{C}_t$ as well as C_t can be calculated by applying the Boltzmann equation to a Knudsen layer [38]; their estimated values are of the order unity. The non-dimensional parameter $E_\infty a/T_0$ is known as Epstein number and it is a small number in practice [39]. The solutions of the field equations (3.3)–(3.5) with the boundary conditions (3.6)–(3.11) are similar to those developed by Li and Keh [33] for the case of axially symmetric thermophoresis of a spherical particle in a spherical cavity filled with a gaseous medium, and are given by

$$T_p = T_0 + E_\infty \sum_{m=0}^{\infty} R_{1m}\, r_1^m\, P_m(\zeta_1), \tag{3.12}$$
$$T = T_0 + E_\infty \sum_{m=0}^{\infty} \Big[S_{1m}\, r_1^{-m-1}\, P_m(\zeta_1) + R_{2m}\, r_2^m\, P_m(\zeta_2) \Big], \tag{3.13}$$
$$T_w = T_0 - E_\infty z + E_\infty \sum_{m=0}^{\infty} S_{2m}\, r_2^{-m-1}\, P_m(\zeta_2), \tag{3.14}$$

where P_m is the Legendre polynomial of order m, and ζ_i is equal to $\cos\theta_i$ with $i = 1$ and 2. Equations (3.12)–(3.14) immediately satisfy the boundary conditions (3.10) and (3.11), and R_{1m}, S_{1m}, R_{2m}, and S_{2m} are unknown constants to be determined from the

remaining boundary conditions. In the expression of the solution in equation (3.13), the superposition of the general solution to the equation (3.4) in spherical coordinates as written from two different origins can be employed due to the linearity of the governing equations. Substituting (3.12)–(3.14) into the boundary conditions (3.6)–(3.9) lead to relations determine the unknown coefficients, we obtain

$$0 = \sum_{m=0}^{\infty} \Big\{ R_{1m} R_m^1(a,\theta_1) + S_{1m} S_m^1(a,\theta_1) + \Big[R_{2m} R_m^2(r_2,\theta_2) \Big]_{r_1=a} \Big\}, \tag{3.15}$$

$$-\tilde{k}_w\, \zeta_2 = \sum_{m=0}^{\infty} \Big\{ \Big[S_{1m} S_m^2(r_1,\theta_1) \Big]_{r_2=b} + R_{2m} R_m^3(b,\theta_2) + S_{2m} S_m^3(b,\theta_2) \Big\}, \tag{3.16}$$

$$0 = \sum_{m=0}^{\infty} \Big\{ R_{1m} R_m^4(a,\theta_1) + S_{1m} S_m^4(a,\theta_1) + \Big[R_{2m} R_m^5(r_2,\theta_2) \Big]_{r_1=a} \Big\}, \tag{3.17}$$

$$-b\, \zeta_2 = \sum_{m=0}^{\infty} \Big\{ \Big[S_{1m} S_m^5(r_1,\theta_1) \Big]_{r_2=b} + R_{2m} R_m^6(b,\theta_2) + S_{2m} S_m^6(b,\theta_2) \Big\}, \tag{3.18}$$

where $\tilde{k}_w = k_w/k_A$ and the definitions of the functions R_m^j and S_m^j with $j = 1, 2 \ldots 6$ are presented by equations (A1)–(A12) in appendix A.

The boundary collocation technique can be employed to enforce equations (3.15)–(3.18) at M points along the semi-circular longitudinal arcs of the particle surface $r_1 = a$ and cavity wall $r_2 = b$ (from $\theta_i = 0$ to $\theta_i = \pi$, where $i = 1$ and 2) and truncate the infinite series in equations (3.12)–(3.14) after M terms, resulting in a system of $4M$ simultaneous linear algebraic equations to be numerically solved to give the $4M$ unknown constants R_{im} and S_{im} with $i = 1$ and 2 for the temperature distribution. This technique can be improved to any degree by taking a sufficiently large value of M.

3.2. Hydrodynamical flow analysis through the porous medium

The field equations governing the slow steady isothermal flow of an incompressible viscous fluid through a porous medium according to Darcy-Brinkman under the Stokesian assumption are given by [40]

$$\nabla \cdot \vec{q} = 0, \tag{3.19}$$

$$\nabla p = \mu\, \nabla^2 \vec{q} - \frac{\mu}{K}\, \vec{q}, \tag{3.20}$$

where $\vec{q}$ is the volume-averaged velocity vector, p is the pore average pressure. The porous medium is characterized by its permeability K which is a measure of the flow conductivity in the porous medium.

The flow generated is axially symmetric and all the hydrodynamic functions are independent of ϕ. Therefore, it is convenient to use the stream function $\psi(r,\theta)$ which is related to the velocity components $q_\rho(r,\theta)$, $q_z(r,\theta)$ in cylindrical coordinates, in the form

$$q_\rho = \frac{1}{\rho}\frac{\partial \psi}{\partial z}, \quad q_z = -\frac{1}{\rho}\frac{\partial \psi}{\partial \rho}. \tag{3.21}$$

Elimination of p from the equation (3.20), it is found that function ψ satisfy the following differential equation

$$L_{-1}(L_{-1}-\alpha^2)\,\psi=0, \tag{3.22}$$

where the axisymmetric Stokes operator L_{-1} is given by

$$L_{-1}=\frac{\partial^2}{\partial\rho^2}-\frac{1}{\rho}\,\frac{\partial}{\partial\rho}+\frac{\partial^2}{\partial z^2}.$$

In this study, we consider the effect of thermal creep, frictional slip, and thermal stress slip along the surface of the particle and the wall cavity [33]. Thus, the boundary conditions for the fluid velocity in porous medium are

$$\vec{q}=U\,\vec{e}_z+\frac{C_s\,\mu}{\rho_A T_0}(\mathbf{I}-\vec{e}_{r_1}\vec{e}_{r_1})\cdot\nabla T+\frac{C_m\,\ell}{\mu}(\mathbf{I}-\vec{e}_{r_1}\vec{e}_{r_1})\cdot\Big[\vec{e}_{r_1}:\Big(\mathbf{t}-\frac{C_h\,\mu^2}{\rho_A T_0}\nabla\nabla T\Big)\Big], \tag{3.23}$$

$$\vec{q}=\frac{\hat{C}_s\,\mu}{\rho_A T_0}(\mathbf{I}-\vec{e}_{r_2}\vec{e}_{r_2})\cdot\nabla T-\frac{\breve{C}_m\,\ell}{\mu}(\mathbf{I}-\vec{e}_{r_2}\vec{e}_{r_2})\cdot\Big[\vec{e}_{r_2}:\Big(\mathbf{t}-\frac{\hat{C}_h\,\mu^2}{\rho_A T_0}\nabla\nabla T\Big)\Big], \tag{3.24}$$

where U is the unknown thermophoretic migration velocity of the spherical particle, $\mathbf{I}$ is the unit dyadic, $\vec{e}_{r_i}$ is the unit normal vector at the solid surface pointing into the porous medium, $\mathbf{t}=-p\,\mathbf{I}+\mu\,[\nabla\vec{q}+(\nabla\vec{q})^t]$ is the stress tensor, $(\nabla\vec{q})^t$ is the transpose of $\nabla\vec{q}$. The temperature gradient, ∇T and $\nabla\nabla T$ can be calculated from the temperature distribution in equation (3.13). $\breve{C}_m$, $\hat{C}_s$ and $\hat{C}_h$ are the frictional slip, thermal creep, and thermal stress slip coefficients at the cavity surface, respectively.

One can easily checked that the solution of equation (3.22), subject to the boundary conditions (3.23) and (3.24), is given by [16,41]

$$\psi=\sum_{n=2}^{\infty}\Big[\Big(A_n r_1^{-n+1}+\sqrt{r_1}\,B_n K_{n-\frac{1}{2}}(\alpha\,r_1)\Big)\mathfrak{I}_n(\zeta_1)+\Big(C_n r_2^{n}+\sqrt{r_2}\,D_n I_{n-\frac{1}{2}}(\alpha\,r_2)\Big)\mathfrak{I}_n(\zeta_2)\Big], \tag{3.25}$$

where I_m and K_m are modified Bessel functions of order m of the first and the second kind, respectively, and $\mathfrak{I}_n$ is the Gegenbauer polynomial of the first kind of order n and degree $-1/2$. The coefficients A_n, B_n, C_n and D_n are unknown constants which will be determined using the boundary conditions at the particle surface and cavity wall.

Using the equation (3.25), the expression for the pressure in the porous medium region is

$$p=-\mu\,\alpha^2\sum_{n=2}^{\infty}\Big[\frac{1}{n}\,A_n r_1^{-n}P_{n-1}(\zeta_1)-\frac{1}{n-1}\,C_n r_2^{n-1}P_{n-1}(\zeta_2)\Big], \tag{3.26}$$

In the construction of the solution in equation (3.25), the general solution to the equation (3.20) in two different spherical coordinate systems are superimposed [41]. Thus, the expressions for the radial and axial velocity components, and the normal and shear stresses in the flow through the porous region are given by

$$q_\rho = \sum_{n=2}^{\infty} \Big[A_n A_{1n}(r_1,\theta_1) + B_n B_{1n}(r_1,\theta_1) + C_n C_{1n}(r_2,\theta_2) + D_n D_{1n}(r_2,\theta_2) \Big], \tag{3.27}$$

$$q_z = \sum_{n=2}^{\infty} \Big[A_n A_{2n}(r_1,\theta_1) + B_n B_{2n}(r_1,\theta_1) + C_n C_{2n}(r_2,\theta_2) + D_n D_{2n}(r_2,\theta_2) \Big], \tag{3.28}$$

$$t_{rr} = \mu \sum_{n=2}^{\infty} \Big[A_n A_{3n}(r_1,\theta_1) + B_n B_{3n}(r_1,\theta_1) + C_n C_{3n}(r_2,\theta_2) + D_n D_{3n}(r_2,\theta_2) \Big], \tag{3.29}$$

$$t_{r\theta} = \mu \sum_{n=2}^{\infty} \Big[A_n A_{4n}(r_1,\theta_1) + B_n B_{4n}(r_1,\theta_1) + C_n C_{4n}(r_2,\theta_2) + D_n D_{4n}(r_2,\theta_2) \Big], \tag{3.30}$$

where the explicit expressions A_{sn}, B_{sn}, C_{sn} and D_{sn} with $s = 1, 2, \ldots 4$ are listed in appendix B.

To determine the unknown constants A_n, B_n, C_n and D_n, we apply the boundary conditions (3.23) and (3.24) at the spherical surfaces, one obtains

$$\sum_{n=2}^{\infty} \Big\{ A_n a_{1n}(a,\theta_1) + B_n b_{1n}(a,\theta_1) + \Big[C_n c_{1n}(r_2,\theta_2) + D_n d_{1n}(r_2,\theta_2) \Big]_{r_1=a} \Big\}$$
$$= \frac{\mu\, E_\infty}{\rho_A\, T_0} \sum_{m=0}^{\infty} \Big\{ S_{1m} S_m^7(a,\theta_1) + \Big[R_{2m} R_m^7(r_2,\theta_2) \Big]_{r_1=a} \Big\} \zeta_1, \tag{3.31}$$

$$\sum_{n=2}^{\infty} \Big\{ A_n a_{2n}(a,\theta_1) + B_n b_{2n}(a,\theta_1) + \Big[C_n c_{2n}(r_2,\theta_2) + D_n d_{2n}(r_2,\theta_2) \Big]_{r_1=a} \Big\}$$
$$= -\frac{\mu\, E_\infty}{\rho_A\, T_0} \sum_{m=0}^{\infty} \Big\{ S_{1m} S_m^7(a,\theta_1) + \Big[R_{2m} R_m^7(r_2,\theta_2) \Big]_{r_1=a} \Big\} \sin\theta_1 + U, \tag{3.32}$$

$$\sum_{n=2}^{\infty} \Big\{ \Big[A_n a_{3n}(r_1,\theta_1) + B_n b_{3n}(r_1,\theta_1) \Big]_{r_2=b} + C_n c_{3n}(b,\theta_2) + D_n d_{3n}(b,\theta_2) \Big\}$$
$$= \frac{\mu\, E_\infty}{\rho_A\, T_0} \sum_{m=0}^{\infty} \Big\{ \Big[S_{1m} S_m^8(r_1,\theta_1) \Big]_{r_2=b} + R_{2m} R_m^8(b,\theta_2) \Big\} \zeta_2, \tag{3.33}$$

$$\sum_{n=2}^{\infty} \Big\{ \Big[A_n a_{4n}(r_1,\theta_1) + B_n b_{4n}(r_1,\theta_1) \Big]_{r_2=b} + C_n c_{4n}(b,\theta_2) + D_n d_{4n}(b,\theta_2) \Big\}$$
$$= -\frac{\mu\, E_\infty}{\rho_A\, T_0} \sum_{m=0}^{\infty} \Big\{ \Big[S_{1m} S_m^8(r_1,\theta_1) \Big]_{r_2=b} + R_{2m} R_m^8(b,\theta_2) \Big\} \sin\theta_2. \tag{3.34}$$

The definitions of the functions a_{sn}, b_{sn}, c_{sn} and d_{sn} (S_m^7, R_m^7, S_m^8 and R_m^8) are also presented in the appendix B (appendix A), respectively.

To determine the fluid velocity components, the boundary conditions (3.31)–(3.34) should be satisfied exactly along the entire surfaces of the sphere and cavity. This results in a linear system of algebraic equations with infinite number of unknown coefficients, which are impossible to solve. However, this difficulty can be avoided if we adopt the boundary collocation method [41]. It first necessitates that the infinite series be truncated after a certain number (N) of terms so that the number of the unknown coefficients become finite. Then, sufficient points on each of the semi-circular longitudinal arcs of the particle

surface and cavity wall are selected as collocation points, where the boundary conditions are enforced to give the same number of linear equations ($4N$) as that of the coefficients. Solving these equations (numerically) subsequently enables one to determine the flow field. In general, more boundary collocation points are required to attain a given accuracy when the particle-to-cavity radius ratio approaches asymptotically to unity and when the relative distance between the centres of the spherical particle and cavity wall is also close to unity. The system of linear algebraic equations ($4N$) to be solved for the constants A_n, B_n, C_n and D_n is constructed from equations (3.31)–(3.34). In order to specify the points along the semi-circular generating arcs of the spherical surfaces where the boundary conditions are exactly satisfied, we have to choose the points $\theta_i = 0$ and $\pi\,(i = 1, 2)$ due to the fact that these points control the extreme gaps between the spherical particle and the cavity surfaces. Additionally, the points $\theta_i = \pi/2$ should be considered. However, an examination of the systems of linear algebraic equations for the unknown constants A_n, B_n, C_n and D_n indicates that the coefficient matrix becomes singular if these points are used. Therefore, to avoid this singular matrix and achieve good accuracy, we follow the method recommended in the literature [33,41] to choose the collocation points as follows. On the half circle $0 \leq \theta_i \leq \pi$ in any meridional plane, $\theta_i = \varepsilon$, $\pi/2 - \varepsilon$, $\pi/2 + \varepsilon$ and $\pi - \varepsilon$ are taken as four basic multipoles, where ε is specified by a small value so that the singularities at $\theta_i = 0$, $\pi/2$, and π can be avoided. The other points are selected as mirror-image pairs about $\theta_i = \pi/2$ which are evenly distributed on the two quarter circles, excluding points of singularity. A Gaussian elimination method is then used to solve the truncated system of equations (3.31)–(3.34) to determine the desired coefficients.

The drag force F_z acting on the spherical particle boundary $r = 1$ by the fluid can be determined from [16,40]:

$$F_z = \pi\,\mu\,a\,\int_0^{\pi}\Big[r^4\sin^3\theta\,\frac{\partial}{\partial r}\Big(\frac{L_{-1}\psi}{r^2\,\sin^2\theta}\Big) - \alpha^2\,r^2\,\sin\theta\,\frac{\partial\psi}{\partial r}\Big]_{r=1}d\theta. \tag{3.35}$$

Substitute for ψ from (3.25) and using the orthogonality properties of $\mathfrak{I}_n(\zeta)$, we obtain

$$F_z = \frac{2}{3}\pi\,a\,\mu\,\alpha^2\Big(A_2 - 2C_2 - 2B_2K_{\frac{3}{2}}(\alpha) - 2D_2I_{\frac{3}{2}}(\alpha)\Big). \tag{3.36}$$

It should be noted here that only the lower coefficients A_2, B_2, C_2 and D_2 contribute to the hydrodynamic drag force of Brinkman medium upon spherical particle in cavity. In fact, the coefficients are the most accurate and the fastest to converge [41].

Since the particle is freely suspended in the confined porous medium, this force must vanish, that is

$$A_2 - 2C_2 - 2B_2K_{\frac{3}{2}}(\alpha) - 2D_2I_{\frac{3}{2}}(\alpha) = 0. \tag{3.37}$$

The thermophoretic migration velocity U of the spherical particle can be obtained by solving equation (3.37) and the $4N$ algebraic equations resulting from equations (3.31)–(3.34) simultaneously.

Due to the linearity of the problem, the migration velocity can be written as the

following decomposition form:

$$U = M_t\, U_0 + M_{0s}\, \hat{C}_s\, \frac{\mu\, E_\infty}{\rho_A\, T_0}. \tag{3.38}$$

where U_0 is the thermophoretic migration velocity of a particle embedded in an unbounded porous medium given from (1.2) and the term $M_{0s}\hat{C}_s\frac{\mu E_\infty}{\rho_A T_0}$ represents the velocity of the particle caused by the recirculation of the thermoosmotic flow due to the presence of the cavity wall. The mobilities M_t and M_{os} are non-dimensional quantities and are, in general, functions of thermal, frictional and geometrical parameters of the problem: the permeability parameter of the porous medium α, slip/jump parameters $\tilde{C}_m$, $\tilde{C}_t$, C_s, C_h, $\hat{C}_m$, $\hat{C}_t$, $\hat{C}_s$ and $\hat{C}_h$, thermal conductivity ratios $\tilde{k}_p$ and $\tilde{k}_w$, eccentricity of the particle position $d/(b-a)$ and particle-to-cavity radius ratio a/b. To obtain the numerical values of the mobilities M_t and M_{os}, it is necessary to explain their physical meaning: M_t represent thermophoretic mobility of the particle within a cavity with $\hat{C}_s = \hat{C}_h = 0$, normalized with respect to U_0, and M_{os} represents the mobility of a particle with $C_s = C_h = 0$ that is with no thermophoretic motion in a cavity including the effect of thermoosmotic flow recirculation coming from the interaction of the thin Knudsen layer around the cavity wall in the presence of temperature gradient; note that M_{os} is normalized with respect to $\mu\hat{C}_s E_\infty/\rho_A T_0$.

For the particular case of an aerosol sphere located at the center of a spherical cavity (i.e., $d/(b-a) = 0$) filled with porous medium, the exact solution of the mobility coefficients M_t and M_{os} has been obtained analytically as [34]

$$M_t = \frac{3\tilde{k}_w\, \vartheta_1\, P}{(\alpha+1)\,\Delta}\Big(\lambda\,(2\hat{C}_m - 1)\,(\beta_6\,\lambda^2 - \beta_2)\,\alpha - \alpha^2\,\beta_1\,\hat{C}_m - 3\beta_1\,(2\hat{C}_m - 1)\,\lambda^2\Big), \tag{3.39}$$

$$M_{os} = \frac{18\tilde{k}_w}{\Delta}\Big(\vartheta_5\,\lambda^2 - \alpha\,\beta_5\,(2\tilde{C}_m + 1)\Big)\Big(P + \lambda^3\,Q - 3\lambda^3\,Q\,\hat{C}_m\,(\hat{C}_h/\hat{C}_s)\Big), \tag{3.40}$$

where $\lambda = a/b$, the expressions for Δ, P, Q, β_j and ϑ_j are also given in appendix B.

4. Numerical results and discussion

The numerical values of the normalized thermophoretic migration velocity U/U_0, and the mobilities coefficients M_t and M_{os} of a spherical particle undergoing axisymmetric thermophoresis within a nonconcentric spherical cavity, filled of porous medium, can be achieved using the boundary collocation method explained in the previous section. The system of linear algebraic equations to be solved for the unknowns R_{1m}, R_{2m}, S_{1m} and S_{2m} is constructed from (3.15)–(3.18), and that for A_n, B_n, C_n and D_n is composed from equations (3.31)–(3.34). Throughout our work in graphing and tabulation, we consider without loss of generality, the typical case of $\tilde{C}_t/\tilde{C}_m = 2$, $\hat{C}_t = \lambda\,\tilde{C}_t$, $\hat{C}_m = \lambda\,\tilde{C}_m$ and $\tilde{k}_w = \tilde{k}_p$ [33,36]. In this manuscript $K_n\,(= \ell/a) = 0$ is used to retrieve the no-frictional slip flow limit [9]. In the limiting case of $K_n \to 0$, the thermophoretic velocity of the particle given by equation (3.38) is proportional to the thermal creep coefficients, the permeability parameter characterizing the porous medium, but do not depend on the jump/slip coefficients.

The collocation solutions for the mobility coefficients M_t and M_{os} defined by equation (3.38) are presented in Table 1 and Figs. 2–7 for various values of the particle-to-cavity size ratio λ, relative center-to-center distance of the particle and cavity $\delta\,(= d/(b-a))$, permeability parameter of the porous medium α, thermal conductivity ratio $\tilde{k}_p$, frictional slip parameter $\tilde{C}_m$, and relative thermal stress slip coefficient C_h/C_s. All the numerical results converge to at least the significant digits as shown in Table 1 with the required numbers of the collocation points M and N. For the difficult cases of $\lambda = 0.99$ and $\delta = 0.96$, the number of collocation points $M(= N)$ is taken 48, which were sufficiently large to attain this convergence. In general, the plots indicate that for the entire range of the permeability parameter, the mobility coefficients M_t and M_{os} are positive, which means that the contributions from the cavity-induced thermoosmotic flow to the particle velocity and from the thermophoretic driving force are in the same direction.

The results in Table 1 and Fig. 2 show that the variation of thermophoretic mobility coefficient, M_t versus particle-to-cavity radius ratio λ. These plots indicate that for the entire range of thermal ratio $\tilde{k}_p$ and frictional slip $\tilde{C}_m$, the mobility M_t is a monotonic decreasing function with λ increases and vanishes in the touching limit $\lambda \to 1$. In general, the mobility coefficient is maximum at the concentric position $\delta = 0$, and increases as the permeability parameter increases. Again, M_t increases with the increase of thermal conductivity ratio $\tilde{k}_p$ and with decrease of frictional slip $\tilde{C}_m$. Plots, also indicate that, in general, M_t has maximum values for the case of no-frictional slip ($\tilde{C}_m = 0$), and also when $\tilde{k}_p \to \infty$ that is the particle with infinite thermal conductivity tends to be isothermal and fails to produce additional temperature gradients at its surface. As expected, M_t has minimum values for the case $\tilde{k}_p = 0$ which means that the particle with vanishing thermal conductivity fails to transfer heat energy, keeping the other parameters fixed. Fig. 3 exhibits the plots of M_t against the permeability parameter characterizing the porous medium α for various values of the particle-to-cavity radius ratio λ, Knudsen number ℓ/a and the eccentricity of the particle position δ. For given values of the particle-to-cavity radius ratio λ and Knudsen number ℓ/a, the mobility M_t has no significant variation as the permeability parameter increases in the interval $\alpha < 1$, sharp increase in $1 < \alpha < 10$ and then reduce to constant values as increases to Darcian limit $\alpha > 10$. Also, in general the plots show maximum values for M_t in the concentric position $\delta = 0$, and agree excellently with the analytical formula (3.39).

Figs. 4–7 and Table 1 indicate the plots of the mobility coefficient M_{os} of a spherical particle in a spherical cavity filled by porous medium with the circulating thermoosmotic flow induced by the imposed temperature gradient defined by equation (3.38). An examination of Fig. 4 illustrates that for the entire range of the permeability parameter and frictional slip, the mobility coefficient M_{os} is a decreasing function of the relative centre-to-centre distance of the particle and cavity. It is interested to note that, in Stokes limit ($\alpha = 0$), for all frictional slip values, the mobility coefficient M_{os} is positive; while for ($\alpha \geq 1$), M_{os} is also positive for the entire range of δ with partial frictional slip $\tilde{C}_m > 0.1$, and has negative values at some values of δ near contact in the particular case of no-frictional slip, $\tilde{C}_m(= \tilde{C}_t/2) = 0$ (see Table 2). Therefore, an increase in the eccentricity of the particle position in the cavity is to reduce or even reverse the cavity-induced thermoosmotic sweeping force on the particle. Fig. 5 exhibits the variation of the mobility coefficient M_{os} versus the permeability parameter α for various values of the particle-

to-cavity size ratio λ, relative centre-to-centre distance of the particle and cavity δ. It indicates that the maximum relative values of M_{os} occur in the Stokes limit ($\alpha = 0$ result of [33]). For low permeability in the range of Darcian limit, the mobility coefficient M_{os} decreases rapidly to zero, regardless of λ and δ, even in the concentric case $\delta = 0$, and it's in good agreement with the with the available analytical solution (3.40). It is noted also that for $\alpha < 1$ and for the entire range of α, M_{os} has no significant change. In Fig. 6, we note that in the Stokes limit $\alpha = 0$, for the entire range of thermal conductivity ratio $\tilde{k}_w$ and δ, the mobility coefficient M_{os} is also a monotonic decreasing function of the size ratio λ; it has maximum values as $\lambda = 0$ and vanishes in the touching limit. Interestingly, For a nonzero α in the entire range of thermal conductivity ratio $\tilde{k}_w$ and δ, the mobility coefficient M_{os} increase to maximum at some value of λ and then decreases to zero near the touching limit of λ. Fig. 7 presents the plot of M_{os} against the Knudsen number ℓ/a for various values of permeability parameter and eccentricity of the particle position. For the entire range of ℓ/a, it can be noted that mobility coefficient M_{os}, in general, decreases with increases in α and δ.

The plots of the dimensionless net thermophoretic velocity U/U_0 of an aerosol particle inside a non-concentric spherical cavity with $\hat{C}_h = C_h$ and $\hat{C}_s = C_s$, calculated from equation (3.38), are presented in Figs. 8 and 9. The plots of U/U_0 versus the radius ratio λ are shown in Fig. 8 for different values of α, ℓ/a, δ, C_h/C_s, $\tilde{k}_p$ and $\tilde{C}_m$. In general for the Stokes limit, U/U_0 decrease monotonically as λ increases; it has its maximum values at $\lambda = 0$ and vanishes in the touching limit $\lambda \to 1$. For non-zero values of α and entire range of δ, the normalized velocity U/U_0 first increases with an increase in λ from a finite value at $\lambda = 0$, attains a maximum at a relatively large value of λ, and then decreases with a further increase in λ to zero as $\lambda \to 1$. In general, and for specified value of λ, U/U_0 increases with an increase of C_h/C_s and a decrease of Knudsen number ℓ/a. A comparison between the plots in Fig. 8 for $\alpha > 0$, it appears that as α increases, the maximum values of U/U_0 are pushed towards of touching limit. Fig. 9 shows the plots that the dimensionless velocity U/U_0 versus the permeability parameter. For $\lambda \leq 0.3$, the normalized velocity U/U_0 decreases with an increase in α from a constant at small value of the permeability parameter α for the entire range of slip frictional coefficient $\tilde{C}_m$; for $\alpha \gg 1$, the position of the particle inside cavity is irrelevant with respect to U/U_0. For $\lambda > 0.3$, the normalized velocity U/U_0 has no significant variation in the interval $\alpha < 1$, increases to maximum and the decrease to constant values in the Darcian limit again irrespective of if its location in the cavity. The plots show also that the values of U/U_0 in the no-frictional slip case are much greater that of the corresponding values for the cases of partial slip.

5. Conclusion

In this article, we used the boundary collocation technique in the quasi-steady limit of small Reynolds and Péclet numbers to study the problem of thermophoretic motion of an aerosol spherical particle located at an arbitrary position within a spherical cavity filled with a porous medium saturated by a viscous fluid. The motion is caused by a prescribed temperature gradient parallel to the line of the particle and cavity centres. At the solid surfaces of the particle and cavity, we considered the effect of the temperature

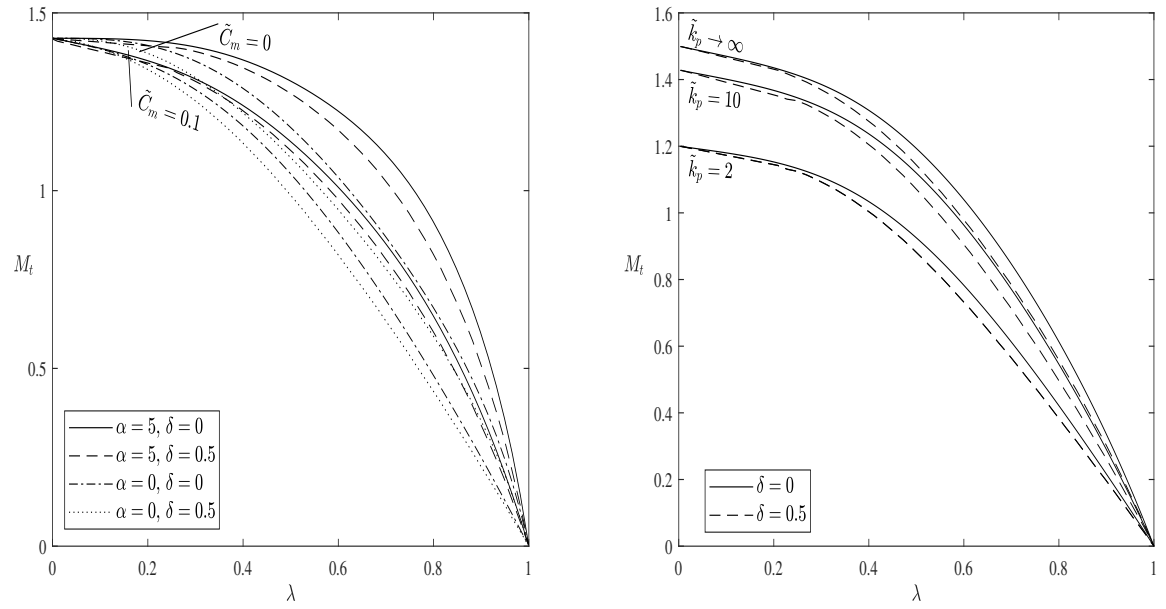

(a) (b)

Fig. 2. Variation of the dimensionless thermophoretic mobility versus the ratio of particle-to–cavity radius λ for different values of α, δ, $\tilde{k}_p$ and $\tilde{C}_m$. Calculations of M_t in (a) with $\tilde{k}_p = 10$ and $C_h/C_s = 0$, and (b) with $\alpha = 2$, $\tilde{C}_m = 0.1$ and $C_h/C_s = 1$.

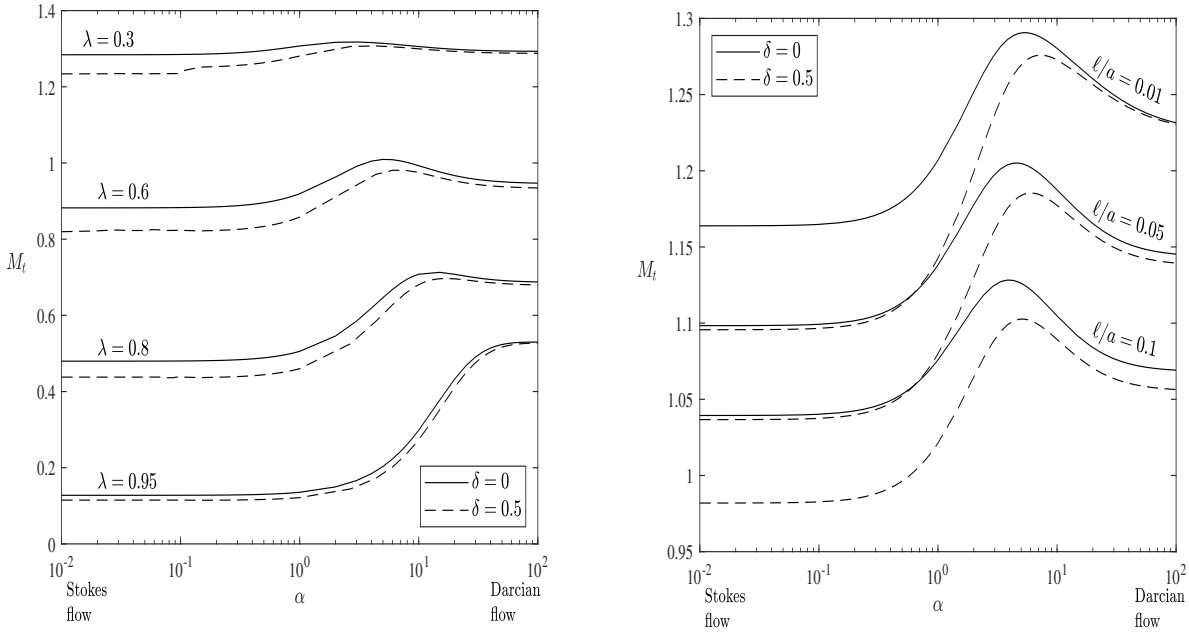

(a) (b)

Fig. 3. Variation of the dimensionless thermophoretic mobility versus the porous parameter α for different values of λ, the Knudsen number ℓ/a and δ with $\tilde{k}_p = 10$ and $C_h/C_s = 1$. Calculations of M_t in (a) with $\tilde{C}_m = 0.1$, and (b) with $\lambda = 0.5$.

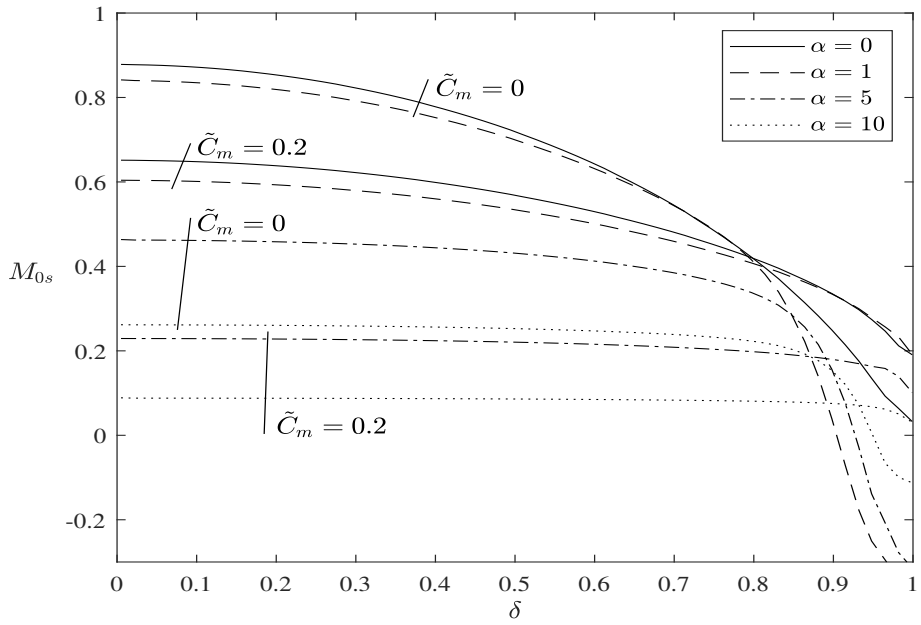

Fig. 4. Variation of the mobility coefficient versus the separation parameter δ for different values of α and $\tilde{C}_m$ with $\tilde{k}_p = 10$, $\lambda = 0.5$ and $\hat{C}_h/\hat{C}_s = 1$.

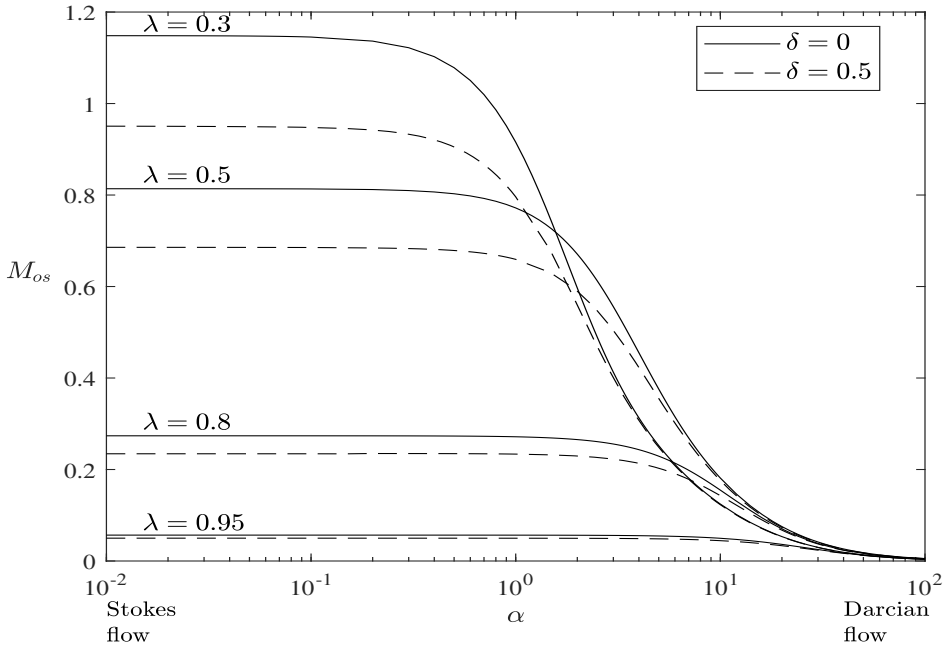

Fig. 5. Variation of the mobility coefficient versus the porous parameter α for different values of λ and δ with $\tilde{k}_p = 10$, $\tilde{C}_m = 0.05$ and $\hat{C}_h/\hat{C}_s = 1$.

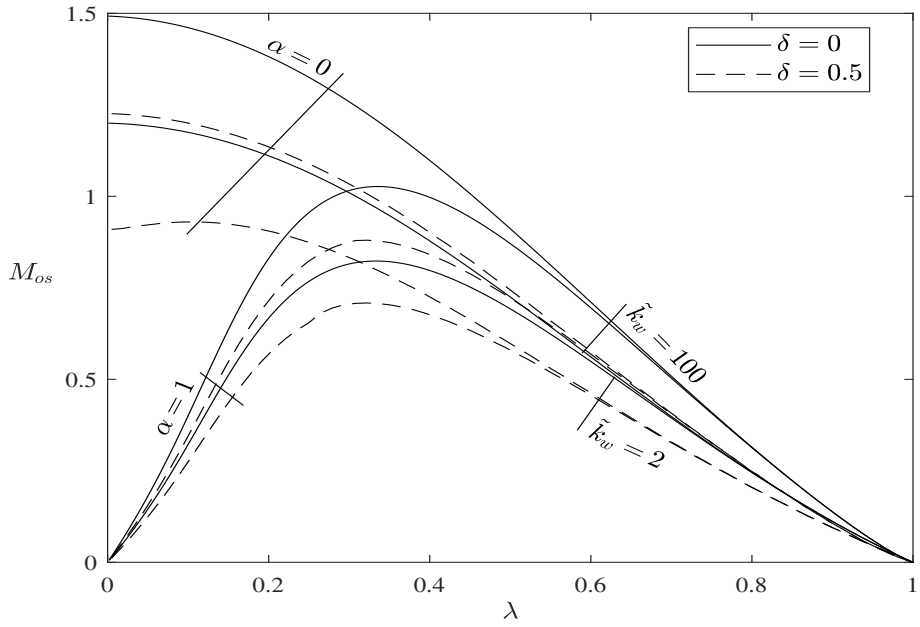

Fig. 6. Variation of the mobility coefficient versus the ratio of particle-to-cavity radius λ for different values of α, $\tilde{k}_w$ and δ with $\tilde{C}_m = 0.01$ and $\hat{C}_h/\hat{C}_s = 0$.

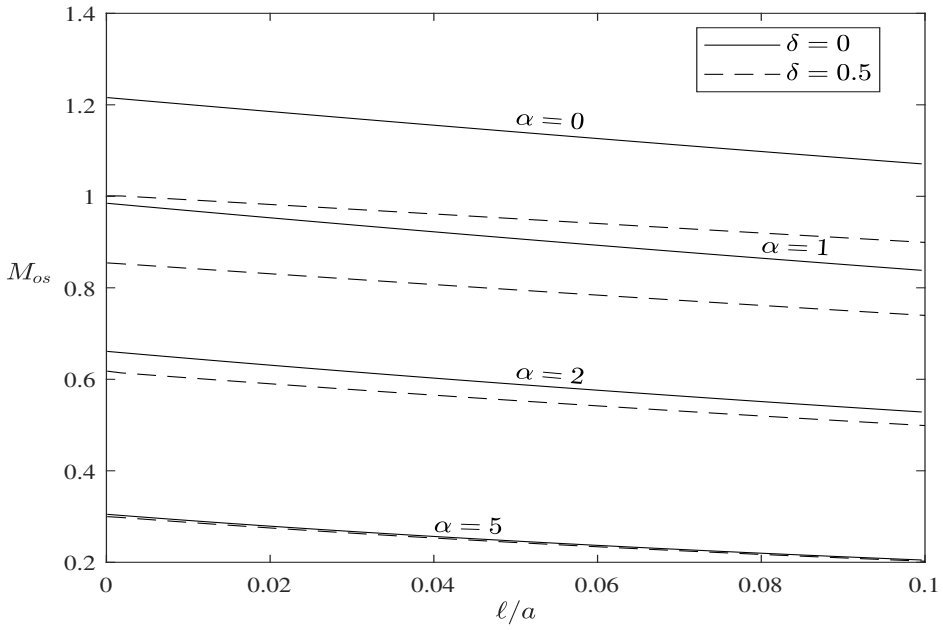

Fig. 7. Variation of the mobility coefficient versus the Knudsen number ℓ/a for different values of α and δ with $\lambda = 0.3$, $\tilde{k}_p = 10$ and $\hat{C}_h/\hat{C}_s = 1$.

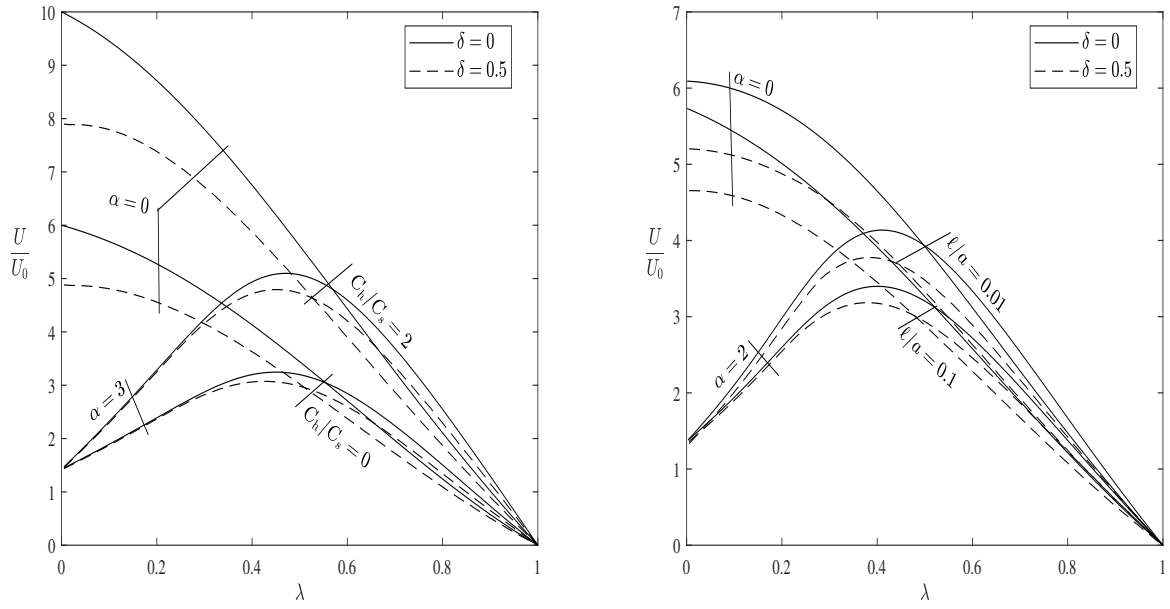

(a) (b)

Fig. 8. Variation of the dimensionless thermophoretic migration velocity versus the ratio of particle-to-cavity radius λ for different values of C_h/C_s, ℓ/a and δ. Calculations of U/U_0 in (a) with $\tilde{k}_p = 10$, $\tilde{C}_m = 0.1$, and (b) with $\tilde{k}_p = 5$.

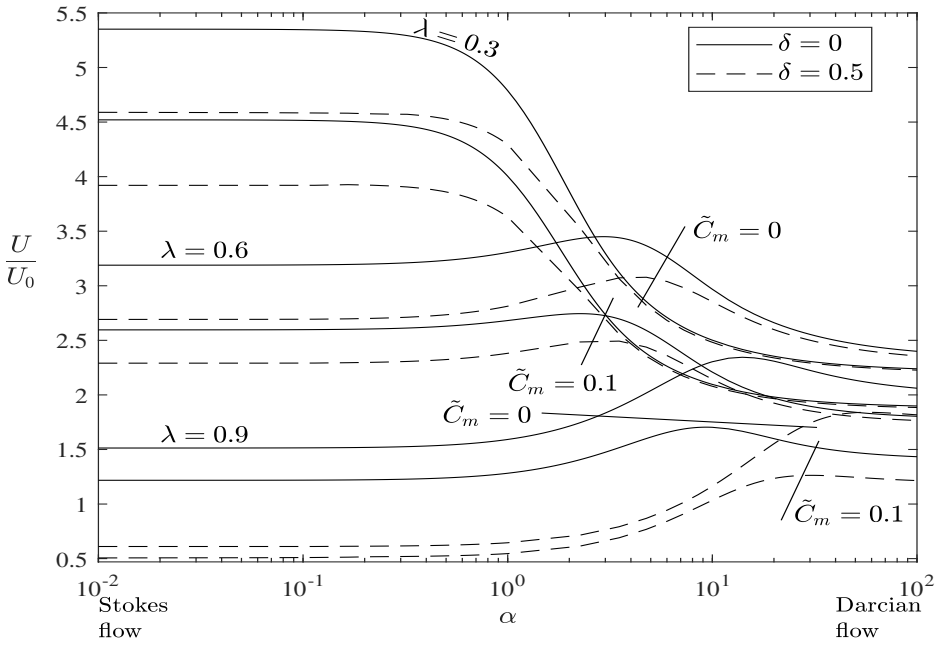

Fig. 9. Variation of the dimensionless thermophoretic migration velocity versus the porous parameter α for different values of λ, δ and $\tilde{C}_m$ with $\tilde{k}_p = 5$.

Table 1
Numerical values of the dimensionless velocity of an eccentric spherical particle undergoing thermophoresis in a spherical cavity at various values of δ and λ with $\alpha = 2$, $\tilde{k}_p = 10$ and $\tilde{C}_m = 0.1$.

δ	λ	M_t		M_{os}		$M = N$
		$\frac{C_h}{C_s} = 0$	$\frac{C_h}{C_s} = 1$	$\frac{\hat{C}_h}{\hat{C}_s} = 0$	$\frac{\hat{C}_h}{\hat{C}_s} = 1$	
0	0.2	1.36739	1.36739	0.36354	0.36362	
	0.4	1.23693	1.23693	0.62378	0.62594	
	0.6	0.96313	0.96313	0.50030	0.50970	
	0.9	0.28983	0.28983	0.10021	0.11288	
	0.99	0.03079	0.03079	0.00839	0.01023	
10E-4	0.2	1.36659	1.36659	0.36549	0.36472	18
	0.4	1.23647	1.23647	0.62259	0.62376	18
	0.6	0.96159	0.96159	0.49864	0.50780	20
	0.9	0.28784	0.28784	0.09975	0.11055	24
	0.99	0.03047	0.03047	0.00830	0.01012	36
0.25	0.2	1.38837	1.38834	0.36816	0.36826	18
	0.4	1.23867	1.23843	0.61502	0.61750	20
	0.6	0.94619	0.94586	0.48349	0.49339	20
	0.9	0.27745	0.27737	0.09530	0.10757	20
	0.99	0.02972	0.02972	0.00809	0.00986	30
0.5	0.2	1.44030	1.43549	0.36889	0.36899	18
	0.4	1.20808	1.20679	0.56802	0.57174	20
	0.6	0.89943	0.89795	0.43517	0.44685	20
	0.9	0.25656	0.25624	0.08625	0.09800	20
	0.99	0.02727	0.02726	0.00740	0.00904	30

jump, frictional slip, thermal creep, and thermal stress slip in the slip flow regime for the gas motion under the assumption of continuum flow. The Brinkman equation is used as a mathematical model for the porous medium. The thermal and hydrodynamic interactions of the cavity wall with the particle surface determine the velocity of the particle given by equations (3.38), (1.2) and their collocation data are obtained for different values of the relative distance between the particle and cavity centres, particle-to-cavity radius ratio, thermal and mechanical properties of the porous-solid system. For the concentric particle-in-cavity case, our results agree excellently with the analytical formula. The wall and permeability of the porous effects on the thermophoretic migration of a particle can be significant in appropriate situations. However, experimental data would be required to confirm the validity of our theoretical work.

Compliance with ethical standards

Conflict of interest: We have no conflict of interest to declare.

Table 2
Numerical values of the mobility coefficient M_{os} for various values of $\tilde{C}_m$, δ, α with $\tilde{k}_p = 10$, $\lambda = 0.5$ and $\hat{C}_h/\hat{C}_s = 1$.

$\tilde{C}_m$	δ	$\alpha = 0$	$\alpha = 1$	$\alpha = 5$	$\alpha = 10$
0	0.88	0.287221	0.140398	0.216635	0.177514
	0.89	0.267957	0.081810	0.184146	0.164809
	0.90	0.247914	0.017276	0.144177	0.148885
	0.91	0.227029	-0.051325	0.095516	0.128889
	0.92	0.205240	-0.120587	0.037638	0.103848
	0.93	0.182494	-0.185489	-0.028322	0.072817
	0.94	0.158774	-0.239750	-0.098238	0.035262
	0.95	0.134168	-0.276612	-0.163791	-0.008102
	0.96	0.109043	-0.289765	-0.212613	-0.053770
0.4	0.88	0.353408	0.350345	0.184200	0.076911
	0.89	0.343761	0.341815	0.181872	0.076144
	0.90	0.333628	0.332768	0.179336	0.075258
	0.91	0.322937	0.323119	0.176561	0.074222
	0.92	0.311589	0.312772	0.173517	0.072989
	0.93	0.299453	0.301619	0.170182	0.071494
	0.94	0.286351	0.289574	0.166567	0.069634
	0.95	0.272024	0.276660	0.162803	0.067246
	0.96	0.256090	0.263363	0.159437	0.064046

References

[1] J. Tyndall, On dust and disease, Proc. R. Inst. 6 (1870) 1-14.

[2] E.H. Kennard, Kinetic Theory of Gases, McGraw-Hill, New York (1938).

[3] S.K. Friedlander, Smoke, Dust and Haze: Fundamentals of Aerosol Behavior, Wiley-Interscience, New York (1977).

[4] A.G.B.M. Sasse, W.W. Nazaroff, A.J. Gadgil, Particle filter based on thermophoretic deposition from natural convection, Aerosol Sci. and Tech. 20 (1994) 227-238.

[5] N. Montassier, D. Boulaud, A. Renoux, Experimental study of thermophoretic particle deposition in laminar tube flow, J. Aerosol Sci. 22 (1991) 677-687.

[6] W.C. Weinberg, Thermophoretic efficiency in modified chemical vapor deposition process, J. Am. Ceram. Soc. 65 (1982) 81-87.

[7] Y. Ye, D.Y.H. Pui, B.Y.H. Liu, S. Opiolka, S. Blumhorst, H. Fissan, Thermophoretic effect of particle deposition on a free standing semiconductor wafer in a clean room, J. Aerosol Sci. 22 (1991) 63-72.

[8] M.M.R. Williams, S.K. Loyalka, Aerosol Science, Theory and Practice, Pergamon Press, Oxford (1991).

[9] G. Karniadakis, A. Beskok, N. Aluru, Microflows and Nanoflows: Fundamentals and Simulation, Springer-Verlag, New York (2005).

[10] C. Shen, Rarefied Gas Dynamics, Springer, Berlin (2005).

[11] E.H. Jones, D.A. Reynolds, A.L. Wood, D.G. Thomas, Use of electrophoresis for transporting nano-iron in porous media, Ground Water 49 (2011) 172-183.

[12] V. Pomès, A. Fernández, D. Houi, Characteristic time determination for transport phenomena during the electrokinetic treatment of a porous medium, Chem. Eng. J. 87 (2002) 251-260.

[13] M.A. Oyanader, P. Arce, A. Dzurik, Design criteria for soil cleaning operations in electrokinetic remediation: Hydrodynamic aspects in a cylindrical geometry, Electrophoresis 26 (2005) 2878-2887.

[14] J.E. Riviere, M.C. Heit, Electrically-assisted transdermal drug delivery, Pharm. Res. 14 (1997) 687-697.

[15] H.C. Brinkman, A calculation of the viscous force exerted by a flowing fluid on a dense swarm of particles, Appl. Sci. Res. A1 (1947) 27-34.

[16] J. Happel, H. Brenner, Low Reynolds Number Hydrodynamics, Martinus Nijoff, The Hague, Netherlands (1983).

[17] R.J. Phillips, W.M. Deen, J.F. Brady, Hindered transport of spherical macro-molecules in fibrous membranes and gels AIChE J. 35 (1989) 1761-1769.

[18] M.S. Faltas, K.E. Ragab, Thermophoretic and photophoretic velocities and forces of a spherical particle embedded in Brinkman medium, Eur. Phys. J. Plus 134 (2019) 475.

[19] L. Talbot, R. Cheng, R. Schefer, D. Willis, Thermophoresis of particles in a heated boundary layer, J. Fluid Mech. 101 (1980) 737-758.

[20] Y. Sone, T. Ohwada, K. Aoki, Temperature jump and Knudsen layer in a rarefied gas over a plane wall: Numerical analysis of the linearized Boltzmann equation for hard-sphere molecules, Phys. Fluids 1 (1989) 363-370.

[21] T. Ohwada, Y. Sone, K. Aoki, Numerical analysis of the shear and thermal creep flows of a rarefied gas over a plane wall on the basis of the linearized Boltzmann equation for hard-sphere molecules, Phys. Fluids 1 (1989) 1588-1599.

[22] S.K. Loyalka, Slip and jump coefficients for rarefied gas flows: variational results for Lennard-Jones and n(r)-6 potentials, Physica A 163 (1990) 813-821.

[23] W.K. Li, C.Y. Soong, C.H. Liu, P.Y. Tzeng, Thermophoresis of a micro-particle in gaseous media with effect of thermal stress slip, Aerosol Sci. Technol. 44 (2010) 1077-1082.

[24] D.A. Lockerby, J.M. Reese, D.R. Emerson, R.W. Barber, Velocity boundary condition at solid walls in rarefied gas calculations, Phys. Rev. E 70 (2004) 017303.

[25] Y.C. Chang, H.J. Keh, Effects of thermal stress slip on thermophoresis and photophoresis, J. Aerosol Sci. 50 (2012) 1-10.

[26] L.J. Wang, H.J. Keh, Boundary effects on thermophoresis of aerosol cylinders, J. Aerosol Sci. 41 (2010) 771-789

[27] L.D. Reed, F.A. Morrison, Particle interactions in low Knudsen number thermophoresis, J. Aerosol Sci. 6 (1975) 349-365.

[28] H.J. Keh, N.Y. Ho, Concentration effects on the thermophoresis of aerosol spheres, J. Colloid Interface Sci. 216 (1999) 167-178.

[29] S.Y. Lu, C.T. Lee, Thermophoretic motion of a spherical aerosol particle in a cylindrical pore, Aerosol Sci. Technol. 37 (2003) 455-459.

[30] H.J. Keh, Y.C. Chang, Thermophoresis of an aerosol sphere perpendicular to two plane walls, AIChE J. 52 (2006) 1690-1704.

[31] C.Y. Li, H.J. Keh, Thermophoresis of a spherical particle in a microtube, J. Aerosol Sci. 113 (2017) 71-84.

[32] E.I. Saad, M.S. Faltas, Theory of thermophoresis of a spherical particle embedded in a micropolar fluid, J. Mol. Liq. 282 (2019) 527-544.

[33] C.Y. Li, H.J. Keh, Axisymmetric thermophoresis of an aerosol particle in a spherical cavity, J. Aerosol Sci. 135 (2019) 33-45.

[34] S. El-Sapa, Effect of permeability of brinkman flow on thermophoresis of a particle in a spherical cavity, Eur. J. Mech. B Fluids 79 (2020) 315-323.

[35] E.I. Saad, M.S. Faltas, Thermophoresis of a spherical particle straddling the interface of a semi-infinite micropolar fluid, J. Mol. Liq. 312 (2020) 113289.

[36] Y.M. Tseng, H.J. Keh, Thermophoretic motion of an aerosol sphere in a spherical cavity, Eur. J. Mech. B Fluids 81 (2020) 93-104.

[37] D.A. Nield, A. Bejan, Convection in Porous Media, third ed., Springer (2006).

[38] F. Sharipov, D. Kalempa, Velocity slip and temperature jump coefficients for gaseous mixtures, IV Temperature jump coefficient, Int. J. Heat Mass Transfer 48 (2005) 1076-1083.

[39] J.B. Young, Thermophoresis of a spherical particle: reassessment, clarification, and new analysis, Aerosol Sci. Technol. 45 (2011) 927-948.

[40] E.I. Saad, Start-up Brinkman electrophoresis of a dielectric sphere for Happel and Kuwabara models, Math. Meth. Appl. Sci. 41 (2018) 9578-9591.

[41] M.S. Faltas, E.I. Saad, Slow motion of a porous eccentric spherical particle-in-cell models, Transp. Porous. Med. 95 (2012) 133-150.

Appendix A

The expressions appearing in equations (3.15)–(3.18) are defined as:

$$R_m^1(r,\theta) = -\tilde{k}_p\, m\, r^{m-1}\, P_m(\zeta), \tag{A1}$$
$$S_m^1(r,\theta) = -(m+1)\, r^{-m-2}\, P_m(\zeta), \tag{A2}$$
$$R_m^2(r,\theta) = r^{m-1}\, \delta_1 \left[\left(m\, r - (2m+1)\, d\, \zeta\right) P_m(\zeta) + d\,(m+1)\, P_{m+1}(\zeta)\right], \tag{A3}$$
$$S_m^2(r,\theta) = -\delta_2\,(m+1)\, r^{-m-2} \left(d\, P_{m+1}(\zeta) + r\, P_m(\zeta)\right), \tag{A4}$$
$$R_m^3(r,\theta) = m\, r^{m-1}\, P_m(\zeta), \tag{A5}$$
$$S_m^3(r,\theta) = \tilde{k}_w\, r^{-m-2}\,(m+1)\, P_m(\zeta), \tag{A6}$$
$$R_m^4(r,\theta) = -r^m\, P_m(\zeta), \tag{A7}$$
$$S_m^4(r,\theta) = r^{-m-1} \left(1 + (m+1)\, \tilde{C'}_t\right) P_m(\zeta), \tag{A8}$$
$$R_m^5(r,\theta) = r^m \left[\left(1 + [(2m+1)\, d\, \zeta - m\, r]\, \delta_1\, \tilde{C'}_t\right) P_m(\zeta) - (m+1)\, d\, \delta_1\, \tilde{C'}_t\, P_{m+1}(\zeta)\right], \tag{A9}$$
$$S_m^5(r,\theta) = r^{-m-1} \left[\left(1 - (m+1)\, r\, \delta_2\, \hat{C'}_t\right) P_m(\zeta) - (m+1)\, d\, \delta_2\, \hat{C'}_t\, P_{m+1}(\zeta)\right], \tag{A10}$$
$$R_m^6(r,\theta) = r^m\,(1 + m\, \hat{C'}_t)\, P_m(\zeta), \tag{A11}$$
$$S_m^6(r,\theta) = -r^{-m-1}\, P_m(\zeta), \tag{A12}$$

where $\tilde{C'}_t = C_t\, \ell/r$, $\hat{C'}_t = \breve{C}_t\, \ell/r$, $\tilde{k}_p = k_p/k_A$, and $\delta_i = (d^2 + r^2 + 2(-1)^i\, d\, r\, \zeta)^{-1/2}$.

We have used the relations

$$r_1 = \left(\rho^2 + (z-d)^2\right)^{1/2}, \quad \cos\theta_1 = \frac{z-d}{r_1}, \quad \sin\theta_1 = \frac{\rho}{r_1}, \tag{A13}$$
$$r_2 = \left(\rho^2 + z^2\right)^{1/2}, \quad \cos\theta_2 = \frac{z}{r_2}, \quad \sin\theta_2 = \frac{\rho}{r_2}. \tag{A14}$$

Also, the functions appearing in equations (3.31)–(3.34) are defined by

$$S_m^7(r,\theta) = -(m+1)\, r^{-m-2} \left[C_h\, C'_m\,(2+m) + C_s\right] \left(\zeta\, P_m(\zeta) - P_{m+1}(\zeta)\right) \csc\theta, \tag{A15}$$
$$\begin{aligned} R_m^7(r,\theta) = r^{m-1} \Big[& \Big(\left[(2m+1)\, d\, \zeta^2 - r\,(m+1)\, \zeta - d\, m\right] \delta_1\, C_s + \big\{ r \left[(4m^2-1)\left(r\,\zeta \right.\right. \\ & \left. + 2d\, \sin^2\theta\right) - d\,(6m^2 + 2m - 1)\big]\, \sin^2\theta - r\,(m+1)\,(r\,\zeta - d)\big]\, \delta_1^2 + m\,(m+1)\,\zeta \\ & \left. - (4m^2-1)\,\zeta\, \sin^2\theta \big\}\, C'_m\, C_h \Big) P_m(\zeta) + (m+1) \Big((r - d\,\zeta)\, \delta_1\, C_s + \big\{ r \left[r - d\,\zeta \right.\right. \\ & \left. \left. + (2m-1)\,(2d\,\zeta - r)\, \sin^2\theta\right] \delta_1^2 + (2m-1)\, \sin^2\theta - m \big\}\, C'_m\, C_h \Big) P_{m+1}(\zeta) \Big] \csc\theta, \end{aligned} \tag{A16}$$
$$\begin{aligned} S_m^8(r,\theta) = (m+1)\, r^{-m-2} \Big[& \Big(\big\{ r\,[2d\,(m+1)\, \sin^2\theta + r\,\zeta + d]\, \delta_2^2 + (m+1)\,\zeta \big\}\, \breve{C'}_m\, \hat{C}_h \\ & - (d + r\zeta)\, \delta_2\, \hat{C}_s \Big) P_m(\zeta) + \Big((d\,\zeta + r)\, \delta_2\, \hat{C}_s - r\,\big((2m+3)\,(2d\,\zeta + r)\, \sin^2\theta \\ & + d\,\zeta + r\big)\, \breve{C'}_m\, \hat{C}_h \Big) P_{m+1}(\zeta) \Big] \csc\theta, \end{aligned} \tag{A17}$$
$$R_m^8(r,\theta) = (m+1)\, r^{m-1} \left(\hat{C}_h\, \breve{C'}_m\,(m-1) + \hat{C}_s\right) \left(P_{m+1}(\zeta) - \zeta\, P_m(\zeta)\right) \csc\theta, \tag{A18}$$

where $C'_m = C_m\, \ell/r$, $\breve{C'}_m = \breve{C}_m\, \ell/r$.

Appendix B

The functions appearing in equations (3.27)–(3.30) are defined as:

$$
\begin{aligned}
A_{1n}(r,\theta) &= -r^{-n-1}(n+1)\,\mathfrak{I}_{n+1}(\zeta)\,\csc\theta, && \text{(B1)}\\
B_{1n}(r,\theta) &= -r^{-3/2}\big((n+1)\,K_{n-\frac{1}{2}}(r\alpha)\,\mathfrak{I}_{n+1}(\zeta)\,\csc\theta + r\alpha\,K_{n-\frac{3}{2}}(r\alpha)\,\mathfrak{I}_n(\zeta)\,\cot\theta\big), && \text{(B2)}\\
C_{1n}(r,\theta) &= -r^{n-2}\big((n+1)\,\mathfrak{I}_{n+1}(\zeta)\,\csc\theta - (2n-1)\,\mathfrak{I}_n(\zeta)\,\cot\theta\big), && \text{(B3)}\\
D_{1n}(r,\theta) &= -r^{-3/2}\big((n+1)\,I_{n-\frac{1}{2}}(r\alpha)\,\mathfrak{I}_{n+1}(\zeta)\,\csc\theta - r\alpha\,I_{n-\frac{3}{2}}(r\alpha)\,\mathfrak{I}_n(\zeta)\,\cot\theta\big), && \text{(B4)}\\
A_{2n}(r,\theta) &= -r^{-n-1}P_n(\zeta), && \text{(B5)}\\
B_{2n}(r,\theta) &= r^{-3/2}\big(r\alpha\,K_{n-\frac{3}{2}}(r\alpha)\,\mathfrak{I}_n(\zeta) - K_{n-\frac{1}{2}}(r\alpha)\,P_n(\zeta)\big), && \text{(B6)}\\
C_{2n}(r,\theta) &= -r^{n-2}\big((2n-1)\,\mathfrak{I}_n(\zeta) + P_n(\zeta)\big), && \text{(B7)}\\
D_{2n}(r,\theta) &= -r^{-3/2}\big(r\alpha\,I_{n-\frac{3}{2}}(r\alpha)\,\mathfrak{I}_n(\zeta) + I_{n-\frac{1}{2}}(r\alpha)\,P_n(\zeta)\big), && \text{(B8)}\\
A_{3n}(r,\theta) &= r^{n-2}\Big(2(n+1) + \frac{r^2\,\alpha^2}{n}\Big)P_{n-1}(\zeta), && \text{(B9)}\\
B_{3n}(r,\theta) &= 2r^{-5/2}\big(r\,\alpha\,K_{n-\frac{3}{2}}(r\alpha) + (n+1)\,K_{n-\frac{1}{2}}(r\alpha)\big)P_{n-1}(\zeta), && \text{(B10)}\\
C_{3n}(r,\theta) &= r^{n-3}\Big(4-2n - \frac{r^2\,\alpha^2}{n-1}\Big)P_{n-1}(\zeta), && \text{(B11)}\\
D_{3n}(r,\theta) &= -2r^{-5/2}\big(r\,\alpha\,I_{n-\frac{1}{2}}(r\alpha) + (n-2)\,I_{n-\frac{1}{2}}(r\alpha)\big)P_{n-1}(\zeta), && \text{(B12)}\\
A_{4n}(r,\theta) &= 2(n^2-1)\,r^{-n-2}\mathfrak{I}_n(\zeta)\,\csc\theta, && \text{(B13)}\\
B_{4n}(r,\theta) &= r^{-5/2}\big(2r\alpha\,K_{n-\frac{3}{2}}(r\alpha) + [r^2\,\alpha^2 + 2(n^2-1)]\,K_{n-\frac{1}{2}}(r\alpha)\big)\mathfrak{I}_n(\zeta)\,\csc\theta, && \text{(B14)}\\
C_{4n}(r,\theta) &= 2n\,(n-2)\,r^{n-3}\mathfrak{I}_n(\zeta)\,\csc\theta, && \text{(B15)}\\
D_{4n}(r,\theta) &= r^{-5/2}\big([r^2\,\alpha^2 + 2n\,(n-2)]\,I_{n-\frac{1}{2}}(r\alpha) - 2r\alpha\,I_{n+\frac{1}{2}}(r\alpha)\big)\mathfrak{I}_n(\zeta)\,\csc\theta. && \text{(B16)}
\end{aligned}
$$

Also, the functions appearing in equations (3.31)–(3.34) are defined by

$$
\begin{aligned}
a_{1n}(r,\theta) &= A_{1n}(r,\theta) - C'_m\,A_{4n}(r,\theta)\,\zeta_1, && \text{(B17)}\\
b_{1n}(r,\theta) &= B_{1n}(r,\theta) - C'_m\,B_{4n}(r,\theta)\,\zeta_1, && \text{(B18)}\\
c_{1n}(r,\theta) &= C_{1n}(r,\theta) - C'_m\,C_{4n}(r,\theta)\,\zeta_1, && \text{(B19)}\\
d_{1n}(r,\theta) &= D_{1n}(r,\theta) - C'_m\,D_{4n}(r,\theta)\,\zeta_1, && \text{(B20)}\\
a_{2n}(r,\theta) &= A_{2n}(r,\theta) + C'_m\,A_{4n}(r,\theta)\,\sin\theta_1, && \text{(B21)}\\
b_{2n}(r,\theta) &= B_{2n}(r,\theta) + C'_m\,B_{4n}(r,\theta)\,\sin\theta_1, && \text{(B22)}\\
c_{2n}(r,\theta) &= C_{2n}(r,\theta) + C'_m\,C_{4n}(r,\theta)\,\sin\theta_1, && \text{(B23)}\\
d_{2n}(r,\theta) &= D_{2n}(r,\theta) + C'_m\,D_{4n}(r,\theta)\,\sin\theta_1, && \text{(B24)}\\
a_{3n}(r,\theta) &= A_{1n}(r,\theta) + \breve{C}'_m\,A_{4n}(r,\theta)\,\zeta_2, && \text{(B25)}\\
b_{3n}(r,\theta) &= B_{1n}(r,\theta) + \breve{C}'_m\,B_{4n}(r,\theta)\,\zeta_2, && \text{(B26)}\\
c_{3n}(r,\theta) &= C_{1n}(r,\theta) + \breve{C}'_m\,C_{4n}(r,\theta)\,\zeta_2, && \text{(B27)}\\
d_{3n}(r,\theta) &= D_{1n}(r,\theta) + \breve{C}'_m\,D_{4n}(r,\theta)\,\zeta_2, && \text{(B28)}\\
a_{4n}(r,\theta) &= A_{2n}(r,\theta) - \breve{C}'_m\,A_{4n}(r,\theta)\,\sin\theta_2, && \text{(B29)}\\
b_{4n}(r,\theta) &= B_{2n}(r,\theta) - \breve{C}'_m\,B_{4n}(r,\theta)\,\sin\theta_2, && \text{(B30)}\\
c_{4n}(r,\theta) &= C_{2n}(r,\theta) - \breve{C}'_m\,C_{4n}(r,\theta)\,\sin\theta_2, && \text{(B31)}\\
d_{4n}(r,\theta) &= D_{2n}(r,\theta) - \breve{C}'_m\,D_{4n}(r,\theta)\,\sin\theta_2. && \text{(B32)}
\end{aligned}
$$

The coefficients appearing in equations (3.39) and (3.40) are defined as

$$\Delta = \big((2\hat{C}_t\,\tilde{k}_w + 2\tilde{k}_w + 1)\,P - 2(2\,\hat{C}_t\,\tilde{k}_w - \tilde{k}_w + 1)\,Q\,\lambda^3\big)\,\big[\hat{C}_m\,(2\lambda^3\,\vartheta_5 + \vartheta_3)\,\alpha^2 + \lambda\,(2\hat{C}_m - 1)\,\big(6(\beta_6 + \beta_5)\,(2\tilde{C}_m + 1)\,\lambda^2 - 2\vartheta_2\,\lambda^3 - \vartheta_4\big)\,\alpha + 3\vartheta_3\,(2\hat{C}_m - 1)\,\lambda^2\big], \quad \text{(B33)}$$

with

$$\beta_1 = I_{\frac{3}{2}}(\alpha)\,K_{\frac{3}{2}}(\lambda^{-1}\alpha) - K_{\frac{3}{2}}(\alpha)\,I_{\frac{3}{2}}(\lambda^{-1}\alpha), \quad \beta_2 = I_{\frac{1}{2}}(\lambda^{-1}\alpha)\,K_{\frac{3}{2}}(\alpha) + I_{\frac{3}{2}}(\alpha)\,K_{\frac{1}{2}}(\lambda^{-1}\alpha),$$
$$\beta_3 = I_{\frac{3}{2}}(\lambda^{-1}\alpha)\,K_{\frac{1}{2}}(\alpha) + I_{\frac{1}{2}}(\alpha)\,K_{\frac{3}{2}}(\lambda^{-1}\alpha), \quad \beta_4 = I_{\frac{1}{2}}(\lambda^{-1}\alpha)\,K_{\frac{1}{2}}(\alpha) - I_{\frac{1}{2}}(\alpha)\,K_{\frac{1}{2}}(\lambda^{-1}\alpha),$$
$$\beta_5 = \lambda^{1/2}\big(I_{\frac{3}{2}}(\alpha)\,K_{\frac{1}{2}}(\alpha) + I_{\frac{1}{2}}(\alpha)\,K_{\frac{3}{2}}(\alpha)\big), \quad \beta_6 = \lambda^{-1/2}\big(I_{\frac{1}{2}}(\lambda^{-1}\alpha)\,K_{\frac{3}{2}}(\lambda^{-1}\alpha) + I_{\frac{3}{2}}(\lambda^{-1}\alpha)\,K_{\frac{1}{2}}(\lambda^{-1}\alpha)\big),$$
$$\vartheta_1 = (\alpha^2 + 9\alpha + 9)\,(2\tilde{C}_m + 1) + \alpha^2\,(\alpha + 1)\,\tilde{C}_m, \quad \vartheta_2 = (\alpha\,\beta_4 + 3\beta_2)\,(2\tilde{C}_m + 1) + \alpha^2\,\tilde{C}_m\,\beta_2,$$
$$\vartheta_3 = (\alpha\,\beta_3 - 9\beta_1)\,(2\tilde{C}_m + 1) - \alpha^2\,\tilde{C}_m\,\beta_1, \quad \vartheta_4 = (\alpha\,\beta_4 + 9\beta_2)\,(2\tilde{C}_m + 1) + \alpha^2\,\tilde{C}_m\,\beta_2,$$
$$\vartheta_5 = (\alpha\,\beta_3 - 3\beta_1)\,(2\tilde{C}_m + 1) - \alpha^2\,\tilde{C}_m\,\beta_1, \quad P = 2\tilde{C}_t\,\tilde{k}_p + \tilde{k}_p + 2,\ Q = \tilde{C}_t\,\tilde{k}_p - \tilde{k}_p + 1.$$